How do volatiles escape their shallow magmatic hearth?

Wim Degruyter[1], Andrea Parmigiani[2,4], Christian Huber[3], Olivier Bachmann[2]

[1]School of Earth and Ocean Sciences, Cardiff University, UK
[2]Department of Earth Sciences, ETH Zürich, Switzerland
[3]Department of Earth, Environmental and Planetary Sciences, Brown University, USA
[4]FlowKit, Route d'Oron 11, 1010 Lausanne, Switzerland

Abstract

Only a small fraction (~1-20%) of magmas generated in the mantle erupt at the surface. While volcanic eruptions are typically considered as the main exhaust pipes for volatile elements to escape into the atmosphere, the contribution of magma reservoirs crystallizing in the crust are likely to dominate the volatile transfer from depth to the surface. Here, we use multiscale physical modeling to identify and quantify the main mechanisms of gas escape from crystallizing magma bodies. We show that most of the outgassing occurs at intermediate to high crystal fraction, when the system has reached a mature mush state. It is particularly true for shallow volatile-rich systems that tend to exsolve volatiles through second boiling, leading to efficient construction of gas channels as soon as the crystallinity reaches ~40-50 vol.%. We, therefore, argue that estimates of volatile budgets based from volcanic activity may be misleading because they tend to significantly underestimate the magmatic volatile flux and can provide biased volatile compositions. Recognition of the compositional signature and volumetric dominance of intrusive outgassing is therefore necessary to build robust models of volatile recycling between the mantle and the surface.

Introduction

Volatile elements (which can be either *dissolved or exsolved* in magmas, see definitions below) have a fundamental control over igneous processes in our planet. They play a role in the temperatures at which rocks melt (or magmas crystallize), affect the mechanical response and rheological properties of magmas (in particular viscosities and densities) in reservoirs and conduits, influence eruptive styles, and carry economically-important elements (e.g., S, Cu, Mo, Au, Ag), environmentally critical gases (CO_2, HCl, SO_2), and pollutants (Hg, F, …) towards the surface of the Earth (Edmonds and Wallace 2017). Their composition and transport to the surface can also provide information about the state of the magma reservoir during volcanic unrests (e.g., Matsuo 1962; Chiodini et al. 2017).

Volatile elements are dissolved in silicate melts at high pressure. They come out of solution (*exsolve*) as magmas decompress while they ascend to shallower depths (first

boiling) or crystallize while they cool during storage, which concentrates the volatiles in the melt to the point of saturation (second boiling, e.g., Candela 1994). Hence, silicic subvolcanic magma reservoirs that are typically crystal-rich (Marsh 1981; Koyaguchi and Kaneko 1999; Huber et al. 2009) and located in the upper 10 km of the crust will ultimately saturate and develop an exsolved gas phase (Tait et al. 1989; Newman and Lowenstern 2002; Wallace 2005; Papale et al. 2006). Once a low-density, low-viscosity Magmatic Volatile Phase (hereafter shortened to MVP) is formed, it can potentially leave its magmatic hearth and rise towards the surface. In this paper we explore the underlying mechanisms and their efficiency as magma evolves from storage conditions to solidification.

As silicic volcanic rocks are generally volatile-rich, while their plutonic counterparts are volatile-poor (Parmigiani et al. 2016), a significant amount of MVP should escape into the atmosphere during crustal storage before magmas reach full solidification. Some of the volatiles are entrained by volcanic eruptions (e.g., unexpectedly high sulphur contents in volcanic plumes betrays the presence of excess volatiles in melt-rich portions of magma reservoirs; Wallace 2001; Soden et al. 2002; Shinohara 2008; Scaillet et al. 2013; Parmigiani et al. 2016; Su et al. 2016. However, as most magmatic rocks never reach the surface (intrusive/extrusive ratios are >10:1 for continental settings (White et al. 2006; Ward et al. 2014; Lipman and Bachmann 2015; Perkins et al. 2016; Tierney et al. 2016) and volcanic eruptions are rare in the lifetime of magmatic provinces, passive degassing during non-erupting periods must volumetrically dominate magma outgassing, as shown by decadal sulphur output into the atmosphere Carn et al. 2017. This paper discusses potential mechanisms to feed this passive degassing.

The separation of an MVP from its host magma reservoir is controlled by a balance between three forces: buoyancy of the MVP caused by its density difference with the melt and crystal phases (gravity), viscous drag between phases and capillary forces (because of interfacial tension between the MVP and the melt). Inertia plays a negligible role on MVP-mush separation under magma reservoir conditions. One can therefore parameterize the relative importance of each force by three dimensionless numbers, the Reynolds number (inertia/viscous forces) which is <<1, the Archimedes number (buoyancy/viscous forces) which identically is << 1 given the high viscosity of the melt. The Bond number (buoyancy/capillary forces) is defined by

$$Bo = \frac{\Delta\rho g D^2}{\sigma} \quad (1)$$

with $\Delta\rho$ the density difference between the melt and the MVP, g the gravitational acceleration, D the bubble diameter, and σ the interfacial tension. For magma reservoir conditions, $\Delta\rho \approx 2000$ kg/m^3, $g = 9.81$ m/s^2, $\sigma \approx 0.07$ N/m, and we estimate the average crystal size to be between 0.5 and 5 mm, generating bubble diameters D of similar sizes. This results in a Bond number that spans a range between 0.07 and 7 (see Parmigiani et al., 2016).

Three possible mechanisms for MVP segregation in the magma reservoir have been identified in the literature (See Fig. 1):

(1) bubble flow at high melt fraction (either as discrete bubbles, or as bubbly plumes; Cardoso and Woods 1999; Parmigiani et al. 2016),
(2) channel flow in a permeable crystal network at intermediate melt fraction (Parmigiani et al. 2011; Oppenheimer et al. 2015), and

(3) capillary trapping at low melt fraction, where large overpressures and crystal repacking or brittle/ductile deformation of the crystal mush are required for the MVP to move (Mungall 2015; Parmigiani et al. 2016; Parmigiani et al. 2017).

Regime 1: High melt fraction - bubbly flow

At high melt fraction, bubbles in magmas tend not to be crowded by crystals, as exsolved fluids are dominantly non-wetting with respect to silicate minerals. Considering a closed-system (no input of MVP from surrounding areas), they are also typically in low abundance (< 10 vol.%), as significant second boiling has not yet been contributing much. Hence, exsolved volatiles are expected to form relatively spherical bubbles and dominantly ascend either as individual bubbles or as bubble plumes / trains under the effect of their buoyancy. As the fraction of bubbles becomes higher than a few percent, a hindering effect of neighboring bubbles starts to kick in (see Faroughi and Huber 2015) and the ascent rate decreases because of hydrodynamic bubble-bubble interactions. Although bubble coalescence can enhance phase separation, it is likely to be inefficient because of the low volume fraction of bubbles and high melt viscosity. Moreover, convective motion within the magma entrains bubbles, which can slow down the outgassing process (e.g., Martin and Nokes 1988; Koyaguchi et al. 1990).

Regime 2: Intermediate melt fraction - channel flow

At intermediate melt fraction, one can expect a higher fraction of exsolved MVP through second boiling, which, coupled to the increasing fraction of crystals, favors coalescence and channelization of the MVP. As vertical MVP channels of significant lengths form by viscous fingering, outgassing can become much faster (Parmigiani et al. 2011; Oppenheimer et al. 2015; Parmigiani et al. 2016; Lindoo et al. 2017). The transport efficiency of the MVP is modulated by the effective permeability of the MVP phase in the 3-phase mush. In essence, intermediate crystallinity provide conditions that are optimal for outgassing because the intrinsic permeability of the crystal mush remains high, and the relative permeability of the MVP, which increases with its pore volume fraction, is intermediate to high as well.

Regime 3: Low melt fraction - capillary fracturing

At low melt fraction, the volume fraction of MVP exsolved in the pore space is likely to be high. At the same time, the sizes of pores and pore throats tend to be significantly smaller at high crystallinity so that the intrinsic permeability decreases significantly from ~10^{-7} m^2 to 10^{-10} m^2 with crystal content increasing from ~40 to 75 vol.% (assuming an average crystal size on the order of mm; see Parmigiani et al. 2017; Fig. 2). The overall effect of the phase proportions is such that the effective permeability of the MVP drops to zero (i.e. bubbles are capillary trapped). Hence, outgassing will happen only after some overpressurization of the system, leading to repacking or deformation (elastic, plastic or brittle) of the crystalline framework (Holtzman et al. 2012; Oppenheimer et al. 2015).

Method

In this study, we use numerical simulations at the pore-scale (lattice Boltzmann or LB calculations; see full method description in Parmigiani et al., 2017) focusing on the stress

balance that regulates MVP mobility in a crystalline environment at average crystal volume fraction (0.39-0.75; characteristic of mushy environment, see Bachmann and Huber 2016). In particular, we emphasize the role of buoyancy versus capillary stresses in a porous medium (made out of a crystalline framework) containing a low-density non-wetting phase (the MVP) and a higher density, wetting phase (the silicate melt). The main goal of our pore-scale calculations is to determine in which conditions the modes of MVP transport switch from bubble flow to channel flow (regime 1 to regime 2) and ultimately to capillary clogging (regime 3).

The outcome of these multiphase porous flow simulations is strongly controlled by the initial spatial and size distribution of bubbles in the porous domain. The proportion of bubbles that are poorly connected to the most efficient flow pathways in the medium dictates, to a large extent, the critical volume fraction of bubbles required to form connected MVP pathways and the relative permeability of the mush to MVP outgassing. In a previous set of simulations (Parmigiani et al., 2017), the initial distribution of bubbles, and their respective size, was set randomly, which limited the validity of the results. For instance, larger pores contain prior to exsolution more dissolved volatiles and offer less resistance to bubble growth than smaller pores. In the present study, we build on the model of Parmigiani et al., 2017, but treat the initial spatial and size distribution of MVP bubbles with a more physically consistent approach using spinodal decomposition.

Spinodal decomposition is a well-studied mechanism in statistical mechanics whereby two phases unmix under the principle of mass conservation and capillary stresses. In this study, it is the melt and MVP that repel each other. The size and position of MVP bubbles derived by the unmixing process results in a spatial and size distribution of bubbles that satisfy mass balance locally, i.e. larger bubbles form where they are the most likely to form. This leads to a more consistent and therefore more accurate initial condition, which translates in improved estimation of critical MVP volume fraction for the formation of connected MVP pathways and relative mush permeability for the MVP.

In detail, the initial condition works as follows. The respective mass fraction of the two phases considered in the spinodal decomposition (i.e. melt and MVP) is a priori defined for each run. Both phases are, initially, homogeneously distributed all around the pore space and locally (i.e. at each grid node of the computational domain) obey a pre-determined mass fraction. We start the simulation by adding a relative fluctuation (or disequilibrium) on the order of 0.1% on the mass fraction of volatiles. This small disequilibrium initiates spontaneous phase separation so that non-wetting MVP bubbles start to grow in the pore space. The growth of these bubbles ceases when the two phases are fully separated, such that the final MVP volume fraction is determined by the initial mass fraction (Fig. 3). In this study, we use a fixed Bond number of 0.5 (see equation (1)), which provides a good approximation for magmatic systems with intermediate crystal size and volume fraction (see Parmigiani et al., 2016, 2017).

In order to assess the efficiency of outgassing on the volatile budget at the scale associated with a magma reservoir, we parameterize the results of the pore-scale LB simulations and implement them in a macro-scale reservoir model (Parmigiani et al. 2017). We use the reservoir model of Degruyter and Huber 2014, expanded to include outgassing

(see the detailed implementation in Parmigiani et al. 2017) as it allows us to directly couple thermal and mechanical evolution of the magma reservoir. The original model assumes a magma chamber that evolves due to magma injection, magma withdrawal, exsolution, and crystallization. The magma chamber loses heat to its surroundings (crystalline mush transitioning to crustal wall-rocks), which responds visco-elastically to volume changes of the chamber. For simplicity, we will not consider magma injection or withdrawal, except for the loss of magmatic volatiles by outgassing, which influences the enthalpy budget of the magma body and therefore the cooling rate of the magma chamber.

As in Parmigiani et al. 2017, we initialize the magma chamber at a lithostatic pressure of 200 MPa, a temperature of 850°C, and a volume of 50 km^3. The initial density of the melt and crystals are 2400 kg m^{-3} and 2750 kg m^{-3}, respectively and they vary less than 1% during a calculation. The heat loss is calculated through an analytical solution of a sphere (magma chamber) at the center of a larger sphere (mush and crustal surroundings) that takes into account the time-dependent temperature variations in the chamber. We assume the following thermal properties for the surroundings, a thermal diffusivity of 10^{-6} m^2 s^{-1}, a specific heat capacity of 1200 J kg^{-1} K^{-1}, and a density of 2500 kg m^{-3}. We explore the difference between a colder and hotter crust, by setting the temperature of the outer shell at 250 °C and 300 °C, respectively. The magma solidifies according to a parameterized melt fraction-temperature curve for a dacitic composition (Huber et al. 2009) with a solidus and liquidus temperature of 700 °C and 1020 °C, respectively.

For these conditions, we track the outgassing efficiency during the thermo-mechanical evolution of the chamber. We start from a total water content of 5.5 wt.%. The water exsolves according to a parameterized solubility model for water in rhyolitic melt (Dufek and Bergantz 2005). We use new closure relationships for outgassing based on the results of the pore-scale LB model that includes spinodal decomposition. The nature of the reservoir model requires a volume-averaged parameterization of the results from the pore-scale model. We determine (i) the critical MVP volume fraction ε_g^{cr} at which channels can form, (ii) the intrinsic permeability of the crystal network k, and (iii) the relative permeability k_r of the MVP as a function of the crystallinity ε_X of the mush.

The critical MVP volume fraction in the LB calculations is determined by the minimum MVP volume fraction at which channels are able to form for a given crystal volume fraction. For Bo=0.5 and crystal volume fraction between 0.39 and 0.7, our pore scale simulations yield a critical MVP volume fraction for the formation of percolating MVP pathways that can be fitted as follows (Fig. 4a):

$$\varepsilon_g^{cr} = 0.7495\varepsilon_X^3 - 0.4268\varepsilon_X^2 - 0.1626\varepsilon_X + 0.1478 \quad (2)$$

Below a crystal volume fraction of 0.39, no channels form as the crystals do no longer form a rigid network and are held in suspension. Above a crystal volume fraction of 0.7, no channels form as the pore space becomes too small and poorly connected. These boundaries are indicated in Fig. 1 by the red curves and define the region for MVP loss by channels. The intrinsic permeability of the crystal network is found from single-phase fluid flow simulations through the crystal matrices. It is identical to that of Parmigiani et al. 2017, as we are using the same porous media and we can use the same equation to describe it:

$$k = 10^{-4}(-0.0534\varepsilon_X^3 + 0.1083\varepsilon_X^2 - 0.0747\varepsilon_X + 0.0176)\ m^2 \quad (3).$$

The relative permeability is determined from the LB calculations at the onset of channel formation. The parameterization is then calculated from linear interpolation of the minimum values with respect to critical volume fraction found with the pore-scale simulation, with the additional constraint of zero relative permeability at a crystal volume fraction below and equal to 0.39 (where bubbly flow is assumed to prevail; Fig. 4b). The latter is to avoid a sharp transition between different outgassing regimes. There is also a dependence of the relative permeability on the MVP volume fraction, but this has a negligible effect on the results. As outgassing is generally able to keep pace with exsolution, the MVP volume fraction remains close to the critical MVP volume fraction up to the point of capillary trapping. This set of closure relationships allow us to estimate the mass flow rate out of the chamber that results from outgassing. This enters into the model description as sink terms in the conservation of mass, water, and enthalpy (Parmigiani et al. 2017).

Results

Our results show that the MVP volume fraction needed to form channels is lower taking into account our improved initial bubble distributions (Fig. 4a). Due to the fact that the formation of large bubbles is favored in the best-connected areas of the porous medium, more of the MVP will be able to participate in the formation of channels. Larger pore spaces contain initially a higher integrated mass of volatiles accessible for bubble growth than small pores. Larger and more mobile bubbles are therefore predominantly formed in large and better-connected pore space leading to a greater efficiency at forming MVP percolating pathways (see Figs. 2 and 3) than expected from a random initial distribution of bubbles. Hence, well-connected pores collect more MVP mass, and stabilize channels at lower MVP volume fraction than found in Parmigiani et al. (2017). However, the general behavior remains similar; the most efficient outgassing regime in terms of rate is still at intermediate crystallinity, in which channels can efficiently form due to the effect of crystal confinement (focusing the MVP into the pore space) but are not easily clogged by capillary forces when the MVP volume fraction and porous medium constrictions become too important at very high crystallinities.

The results from the magma reservoir model suggest that although more MVP can be lost earlier (lower crystal content) than what was predicted by Parmigiani et al. (2017), the relative contribution of each outgassing regime (bubble migration, MVP channel formation and capillary fracturing) remains roughly similar (Fig. 5). We estimate the mass fraction of MVP that is released in each regime to be:

- up to 0.05 wt.% of MVP or about 1 % of the total MVP available is lost through migration of bubbles at low crystallinity
- up to ~2.7 wt.% of MVP or about 50% of the total MVP available is lost by channels at intermediate to high crystallinity
- a minimum of ~2.8 wt.% of MVP or about 50% of the total MVP either remains trapped or potentially leaves the chamber through capillary fracturing at high crystallinity.

The elastic response of the surrounding crust will act to hinder outgassing (Fig. 5). When the crust responds elastically, outgassing creates an underpressure in the chamber up to a point where the lithostatic pressure of the surroundings will oppose the buoyancy that

drives the MVP upward (Parmigiani et al. 2017). This underpressure is avoided if the crust responds viscously. Thus, the most efficient outgassing takes place in a large reservoir that sits in a thermally mature crust. Those values are very similar to those proposed by Parmigiani et al (2017), where the results indicated a minimum of 3.25 wt.% of MVP was left behind at high crystallinity. Thus, MVP loss by channels is slightly more efficient when incorporating spinodal decomposition. The minimum amount of H_2O that is left behind (~ 2.8 wt.% H_2O) is independent of the initial total MVP mass fraction as the saturation limit is entirely determined by the critical MVP volume fraction. Hence, systems that are more water-rich than what we started with (5.5 wt.% H_2O) can outgas even more at intermediate crystallinities.

Discussion/outlook

The loss of MVP from shallow maturing magma reservoirs has deep implications for the subsequent thermal evolution of the system as well as the potential and magnitude of forthcoming eruptions. More specifically, because the MVP has a low viscosity, low density, and high compressibility, it can deeply influence the mechanical behavior of magma reservoirs (Huppert and Woods 2002; Pistone et al. 2012). As such the rate of outgassing of magma reservoirs influences the response of magma reservoirs to magma recharges, because the compressibility of the MVP can dampen the pressurization and help such reservoirs to grow rather than blow (e.g., Huppert and Woods 2002; Degruyter et al. 2016). Dampening pressurization by enhanced compressibility can also foster more efficient reheating in the reservoir, potentially leading to a less explosive eruptive style if the system does erupt (Degruyter et al. 2017). Moreover, the fact that melt-rich pockets tend to outgas more slowly than crystal-rich areas leads to MVP accumulation in such melt-rich pockets, fostering larger eruptions due to the increase in compressibility (Huppert and Woods 2002, Parmigiani et al., 2016, Degruyter et al. 2017).

Apart from those mechanical effects on magma reservoir dynamics and volcanic behavior, the presence of an MVP, and the dynamics of outgassing, controls the rates and compositions of gases that escape magmatic systems. As the composition of gases emitted during and in between eruptive events are key to monitor active volcanic areas (Marini et al. 1993; Chiodini et al. 2003; Caliro et al. 2007; Paonita et al. 2016; De Siena et al. 2017), and feed into global volatile cycles on Earth (Hilton et al. 2002; Wallace 2005; Shinohara 2013; Mason et al. 2017), it is of paramount importance to determine how such rates and compositions might evolve as outgassing proceeds in crystallizing magma bodies

1. Rates: In light of our results and assuming a intrusive:extrusive mass ratio of about 10:1 to >50:1 in continental acs (Ward et al. 2014; Lipman and Bachmann 2015; Tierney et al. 2016, White et al. 2006), we expect that volcanic eruptions contributes only a small fraction (a few %, even assuming some MVP accumulation in eruptible pockets of magmas) of the volatile flux from the mantle to the surface at present. The rest of the flux is divided between channel outgassing at intermediate crystallinity (i.e. $0.4 \leq \varepsilon_x \leq 0.7$) and capillary fracturing during the last gasps of the crystallization of plutons (potentially leading to the formation of aplite and pegmatites). Hence, the background volatile flux released at subduction zones is likely dominated by passive outgassing from shallow reservoirs with intermediate

to high crystallinities (> 40 vol.% crystals) with a superimposed lower amplitude perturbation associated with volcanic eruptions (e.g., Carn et al., 2017).

2. Composition: The differences between "low-crystallinity" and "high-crystallinity" outgassing will influence the chemistry of the gases released. For instance, volatile species that have low solubility in silicate melts, or are compatible with the MVP (sulfur species, CO2, Ar, N_2, Cl,…) are likely to partition early into the MVP and outgas predominantly during spikes of volcanic activity. In contrast, less MVP-compatible species (e.g., F, Br, and potentially He and Li) are expected to be dominantly released passively from high-crystallinity bodies. This suggests that constraining the mass and composition of volatile species from eruptive episodes at subduction zones can be misleading not only in terms of the magnitude of the flux, but also the composition of the volatile species involved. For example, CO_2 degasses early (low crystal content), whereas He, which tends to be more soluble than other inert gases (Paonita 2005), may be enriched during degassing at higher crystal content. In consequence, we expect gases emitted during volcanic eruptions to record a bias towards lower He/X (where X=CO_2, N_2, other noble gases) compared to the more abundant high-crystallinity outgassing. The poorly recognized role of intrusive magmas on volatile cycles begs to reassess our understanding of volatile recycling fluxes at subduction zones, both in terms of magnitude and volatile composition. Gas compositions emitted during volcanic eruptions, which are commonly used as a proxy for the Earth's degassing patterns, may not provide an accurate chemical signature for and/or magnitude of the volatiles exchanged between mantle and surface.

Acknowledgements

We would like to thank the organizers of the 2017 Royal Society Hooke meeting on Magma reservoir architecture and dynamics (M. Edmonds, K. Cashman, M. Holness and M. Jackson) for stimulating our community to think about those fascinating issues. During the course of the writing of this paper, O. Bachmann was supported by Swiss NSF grant #200020_165501 and 200021_178928, and C. Huber was supported by an NSF CAREER grant. We thank S. Leclaire, main author of the LB recoloring method implementation in Palabos. We thank K. Cashman, C. Miller and an anonymous reviewer for suggestions to improve this paper.

Figure captions

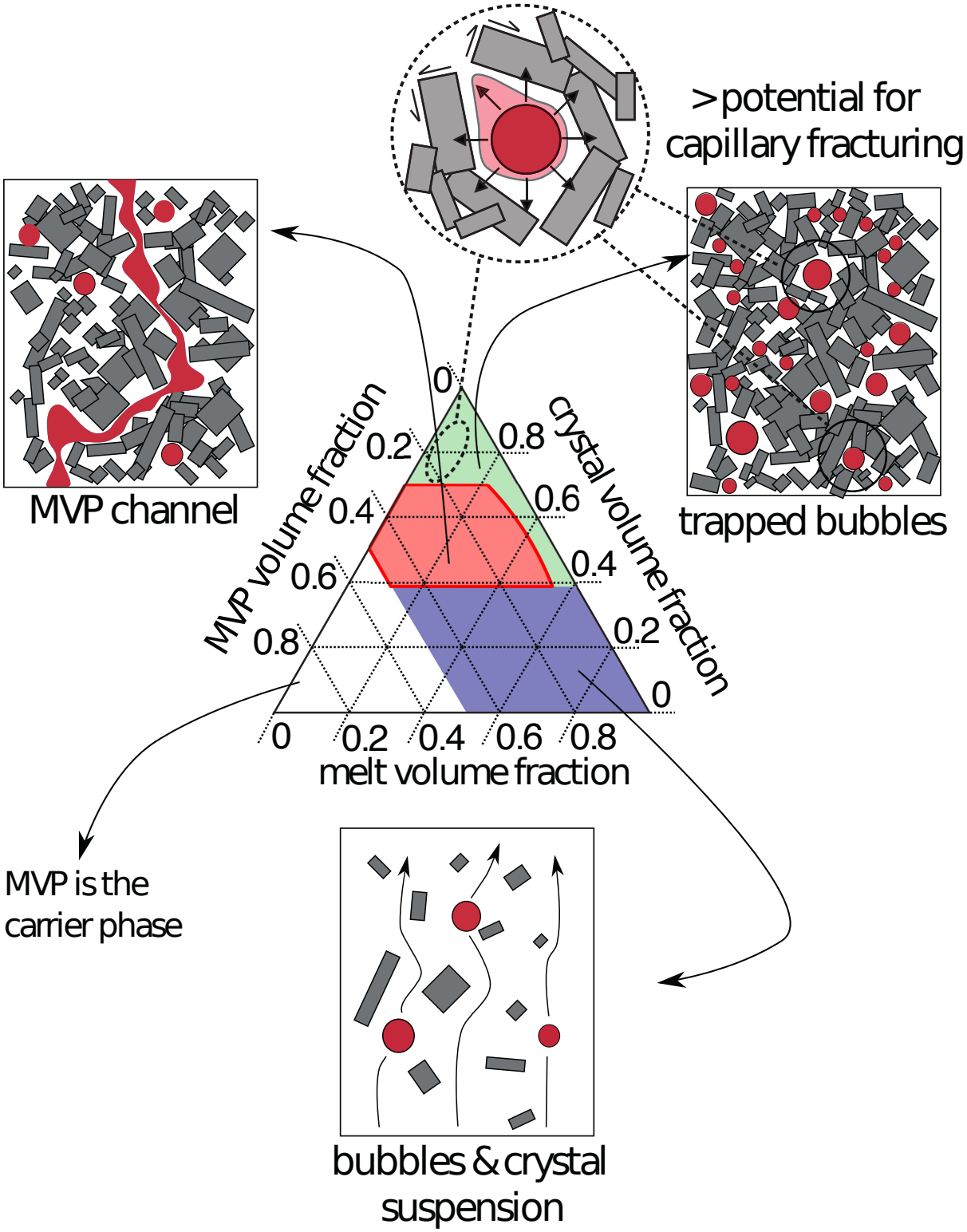

Figure 1: Ternary diagram showing the three possible regimes for outgassing in shallow, silicic magma reservoirs; (1) bubble (and crystal) suspension, (2) MVP channels, and (3) capillary fracturing. The white region where the gas phase is dominant is possible during syn-eruptive outgassing, but is not a mechanism that will operate within the magma reservoir. Modified from Parmigiani et al., 2017.

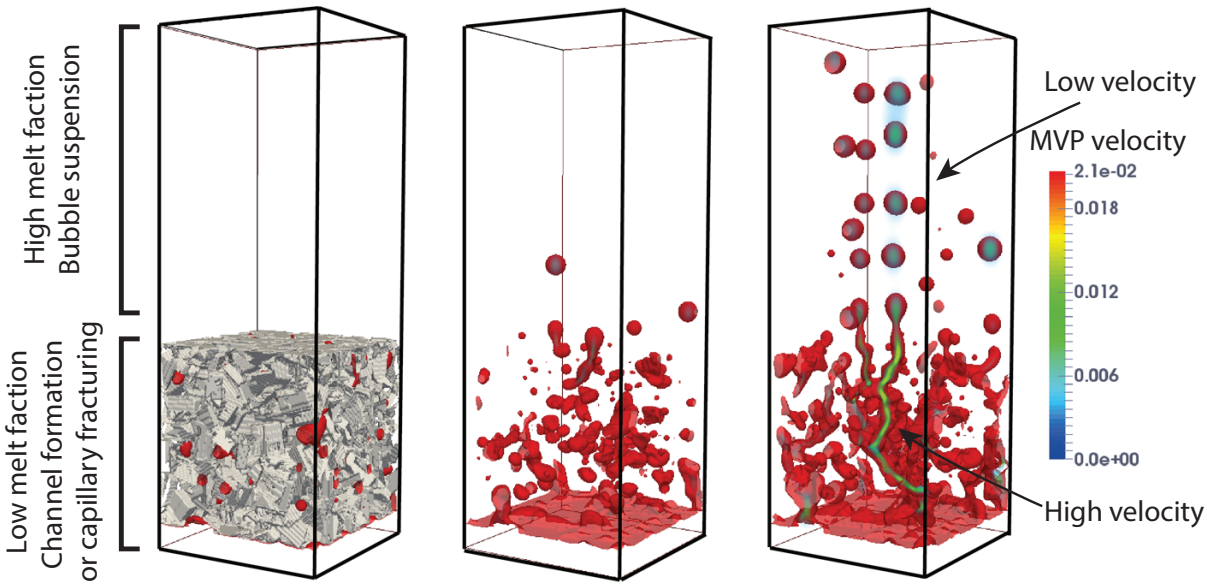

Figure 2: Three different snapshots of the LB numerical simulations. The left panel shows the initial condition. A high melt fraction region overlies a low melt fraction region with the crystal network shown in grey. The dark red color indicates the surface of the MVP. MVP is injected into the bottom of the computational domain. The middle and right panel show the MVP migration over time where the crystal network has been made transparent to be able to visualize the MVP in detail. The velocity field (in lattice units) is also visualized on top of the MVP surfaces with blue indicating low velocity, and red showing high velocity. Once the channels become connected in the low melt fraction region, the velocity of the MVP becomes markedly higher than that in the high melt fraction region, which is dominated by bubble rise.

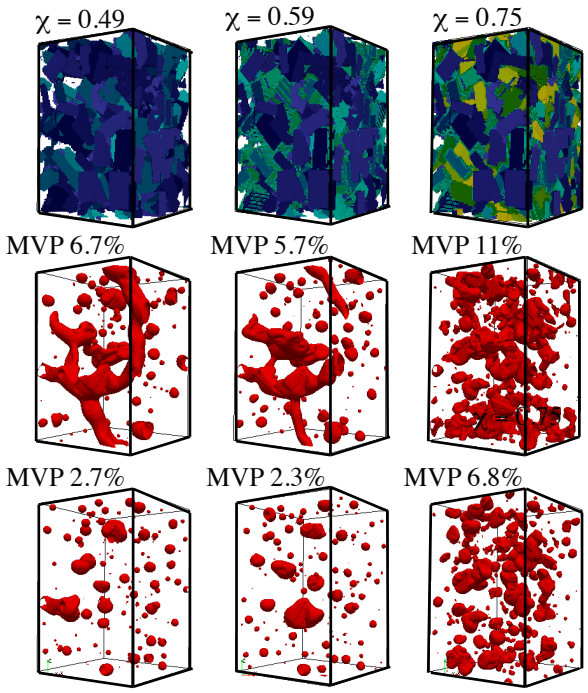

Figure 3: The top panels show the modeled crystal networks used for the LB numerical simulations at three different crystal volume fractions varying from 0.49 to 0.75. The crystals are color-coded dark blue, turquoise and yellow as a visual aid. The six panels on the middle and bottom row show different snapshots of simulations showing the potential spatial distribution of the MVP (in dark red) at different volume fraction (from 2.7 to 11 %) in partially crystallized porous media (the corresponding crystal network shown in the same column is made transparent in these panels to be able to visualize the MVP). Second row: at lower crystal volume fraction values (0.49 and 0.59), MVP concentrations higher than 6% allow MVP channels to form. At higher crystal volume fraction (0.75) the lower degree of connectivity prevents MVP channels to form even at MVP concentration as high as 11%. Third row: bubble distribution for lower MVP volume fractions. MVP volume fraction is too low for MVP channels to form.

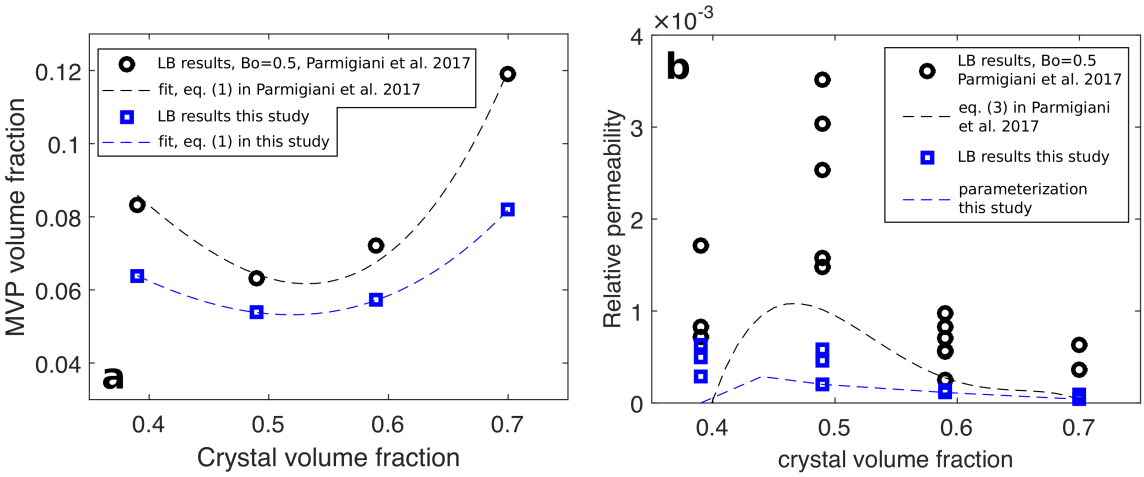

Figure 4: Critical MVP volume fraction (a) and relative permeability (b) for gas channels to form based on lattice Boltzmann simulations (points) of Parmigiani et al. 2017 in black and the current study in blue. The dashed lines show the of ization these results, which were implemented in the reservoir model.

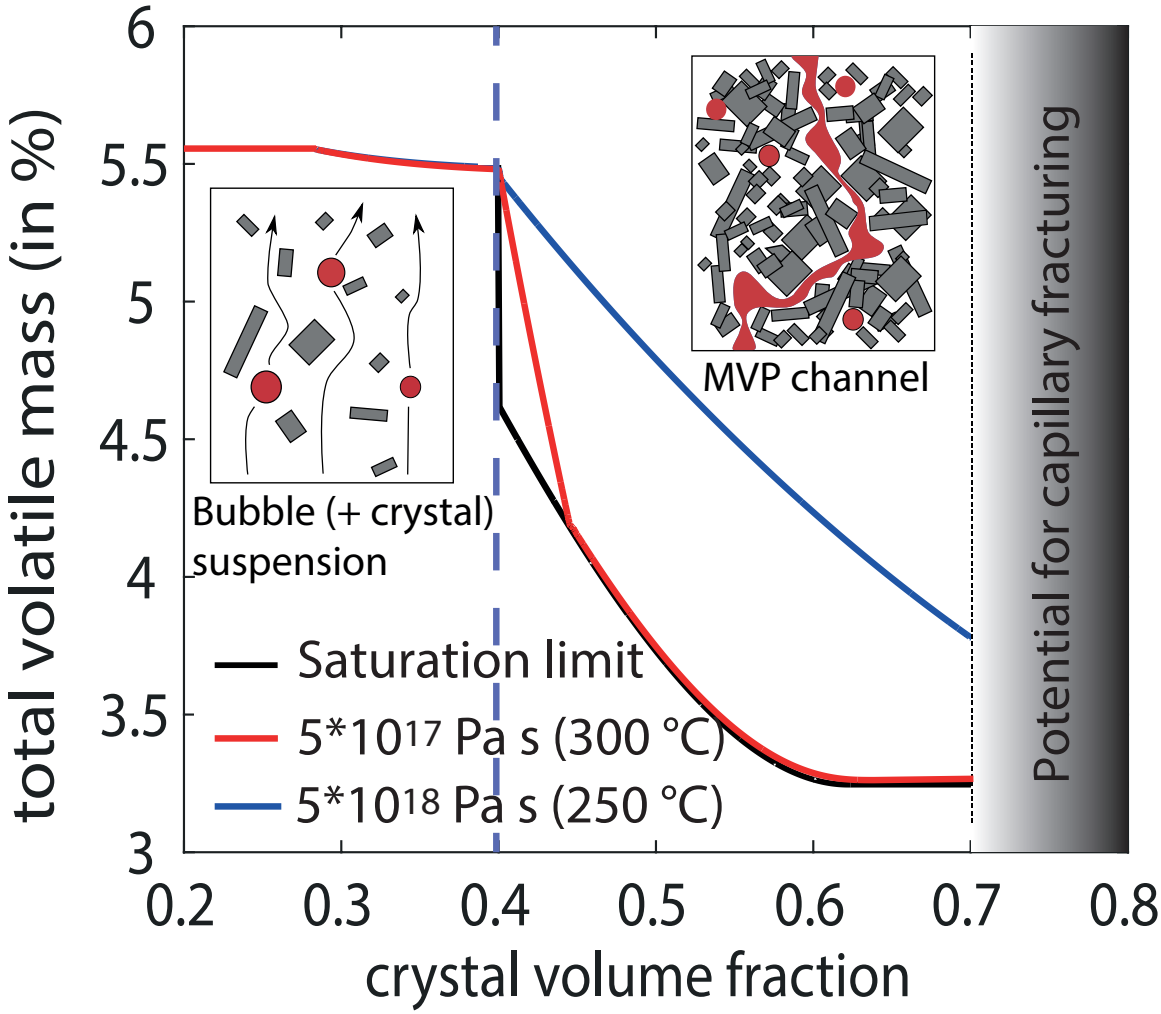

Figure 5: Example of a reservoir scale simulation showing the total amount of MVP loss for the different regimes with different viscosities (and therefore response timescales) for the wall rocks. At high melt fraction, MVP mass loss is negligible, while it is significant in the lower melt fraction regime (total volatile mass fraction goes from about 5.5 to < 3 wt% in this particular case).

References

Bachmann O, Huber C (2016) Silicic magma reservoirs in the Earth's crust. American Mineralogist 101:2377-2404

Caliro S, Chiodini G, Moretti R, Avino R, Granieri D, Russo M, Fiebig J (2007) The origin of the fumaroles of La Solfatara (Campi Flegrei, South Italy). Geochimica et Cosmochimica Acta 71(12):3040-3055 doi:https://doi.org/10.1016/j.gca.2007.04.007

Candela PA (1994) Combined Chemical and Physical Model for Plutonic Devolatilization - a Non-Rayleigh Fractionation Algorithm. Geochimica Et Cosmochimica Acta 58(10):2157-2167

Cardoso SSS, Woods AW (1999) On convection in a volatile-saturated magma. Earth and Planetary Science Letters 168:301-310

Carn SA, Fioletov VE, McLinden CA, Li C, Krotkov NA (2017) A decade of global volcanic SO2 emissions measured from space. Scientific Reports 7:44095 doi:10.1038/srep44095
https://www.nature.com/articles/srep44095#supplementary-information

Chiodini G, Giudicepietro F, Vandemeulebrouck J, Aiuppa A, Caliro S, De Cesare W, Tamburello G, Avino R, Orazi M, D'Auria L (2017) Fumarolic tremor and geochemical signals during a volcanic unrest. Geology

Chiodini G, Todesco M, Caliro S, Del Gaudio C, Macedonio G, Russo M (2003) Magma degassing as a trigger of bradyseismic events: The case of Phlegrean Fields (Italy). Geophysical Research Letters 30(8):n/a-n/a doi:10.1029/2002GL016790

De Siena L, Chiodini G, Vilardo G, Del Pezzo E, Castellano M, Colombelli S, Tisato N, Ventura G (2017) Source and dynamics of a volcanic caldera unrest: Campi Flegrei, 1983–84. Scientific Reports 7(1):8099 doi:10.1038/s41598-017-08192-7

Degruyter W, Huber C (2014) A model for eruption frequency of upper crustal silicic magma chambers. Earth and Planetary Science Letters 403(0):117-130 doi:http://dx.doi.org/10.1016/j.epsl.2014.06.047

Degruyter W, Huber C, Bachmann O, Cooper KM, Kent AJR (2016) Magma reservoir response to transient recharge events: The case of Santorini volcano (Greece). Geology 44(1):23-26 doi:10.1130/G37333.1

Degruyter W, Huber C, Bachmann O, Cooper KM, Kent AJR (2017) Influence of Exsolved Volatiles on Reheating Silicic Magmas by Recharge and Consequences for Eruptive Style at Volcán Quizapu (Chile). Geochemistry, Geophysics, Geosystems 18(11):4123-4135 doi:10.1002/2017GC007219

Dufek J, Bergantz GW (2005) Lower Crustal Magma Genesis and Preservation: a Stochastic Framework for the Evaluation of Basalt–Crust Interaction. Journal of Petrology 46:2167-2195

Edmonds M, Wallace PJ (2017) Volatile and exsolved vapor in volcanic systems. Elements 13:29-34

Faroughi SA, Huber C (2015) Unifying the relative hindered velocity in suspensions and emulsions of nondeformable particles. Geophysical research Letters 42(1):2014GL062570 doi:10.1002/2014gl062570

Hilton DR, Fischer TP, Marty B (2002) Noble Gases and Volatile Recycling at Subduction Zones. Reviews in Mineralogy and Geochemistry 47(1):319-370 doi:10.2138/rmg.2002.47.9

Holtzman R, Szulczewski ML, Juanes R (2012) Capillary Fracturing in Granular Media. Physical Review Letters 108(26):264504

Huber C, Bachmann O, Manga M (2009) Homogenization processes in silicic magma chambers by stirring and mushification (latent heat buffering). Earth and Planetary Science Letters 283(1-4):38-47 doi:10.1016/J.Epsl.2009.03.029

Huppert HE, Woods AW (2002) The role of volatiles in magma chamber dynamics. Nature 420(6915):493-495

Koyaguchi T, Hallworth MA, Huppert HE, Sparks RSJ (1990) Sedimentation of particles from a convecting fluid. Nature 343(6257):447-450

Koyaguchi T, Kaneko K (1999) A two-stage thermal evolution model of magmas in continental crust. Journal of Petrology 40(2):241-254

Lindoo A, Larsen JF, Cashman KV, Oppenheimer J (2017) Crystal controls on permeability development and degassing in basaltic andesite magma. Geology 45(9):831-834 doi:10.1130/G39157.1

Lipman PW, Bachmann O (2015) Ignimbrites to batholiths: Integrating perspectives from geological, geophysical, and geochronological data. Geosphere 11(3) doi:10.1130/ges01091.1

Marini L, Principe C, Chiodini G, Cioni R, Fytikas M, Marinelli G (1993) Hydrothermal eruptions of Nisyros (Dodecanese, Greece). Past events and present hazard. Journal of Volcanology and Geothermal Research 56(1,Äì2):71-94 doi:10.1016/0377-0273(93)90051-r

Marsh BD (1981) On the crystallinity, probability of occurrence, and rheology of lava and magma. Contributions to Mineralogy and Petrology 78:85-98

Martin D, Nokes R (1988) Crystal settling in vigorously convecting magma chamber. Nature 332(7):534-536

Mason E, Edmonds M, Turchyn AV (2017) Remobilization of crustal carbon may dominate volcanic arc emissions. Science 357(6348):290

Matsuo S (1962) Establishment of chemical equilibrium in the volcanic gas obtained from the lava lake of Kilauea, Hawaii. Bulletin Volcanologique 24(1):59-71 doi:10.1007/bf02599329

Mungall JE (2015) Physical Controls of Nucleation, Growth and Migration of Vapor Bubbles in Partially Molten Cumulates. In: Charlier B, Namur O, Latypov R, Tegner C (eds) Layered Intrusions, vol. Springer Netherlands, Dordrecht, pp 331-377

Newman S, Lowenstern JB (2002) VolatileCalc: a silicate melt-H2O-CO2 solution model written in Visual Basic for excel. Computers & Geosciences 28(5):597-604

Oppenheimer J, Rust AC, Cashman KV, Sandnes B (2015) Gas migration regimes and outgassing in particle-rich suspensions. Frontiers in Physics 3 doi:10.3389/fphy.2015.00060

Paonita A (2005) Noble gas solubility in silicate melts:a review of experimentation and theory, and implications regarding magma degassing processes. Annals of Geophysics; Vol 48, No 4-5 (2005) doi:10.4401/ag-3225

Paonita A, Caracausi A, Martelli M, Rizzo AL (2016) Temporal variations of helium isotopes in volcanic gases quantify pre-eruptive refill and pressurization in magma reservoirs: The Mount Etna case. Geology 44(7):499-502 doi:10.1130/G37807.1

Papale P, Moretti R, Barbato D (2006) The compositional dependence of the saturation surface of H2O+CO2 fluids in silicate melts. Chemical Geology 229(1-3):78-95

Parmigiani A, Degruyter W, Leclaire S, Huber C, Bachmann O (2017) The mechanics of shallow magma reservoir outgassing. Geochem Geophys Geosyst 18:2887–2905 doi:10.1002/2017GC006912

Parmigiani A, Faroughi S, Huber C, Bachmann O, Su Y (2016) Bubble accumulation and its role in the evolution of magma reservoirs in the upper crust. Nature 532(7600):492-495 doi:10.1038/nature17401

Parmigiani A, Huber C, Bachmann O, Chopard B (2011) Pore-scale mass and reactant transport in multiphase porous media flows. Journal of Fluid Mechanics 686:40-76 doi:Doi 10.1017/Jfm.2011.268

Perkins JP, Ward KM, de Silva SL, Zandt G, Beck SL, Finnegan NJ (2016) Surface uplift in the Central Andes driven by growth of the Altiplano Puna Magma Body. Nature Communications 7:13185 doi:10.1038/ncomms13185

Pistone M, Caricchi L, Ulmer P, Burlini L, Ardia P, Reusser E, Marone F, Arbaret L (2012) Deformation experiments of bubble- and crystal-bearing magmas: Rheological and

microstructural analysis. Journal of Geophysical Research: Solid Earth 117(B5):B05208 doi:10.1029/2011jb008986

Scaillet B, Luhr JF, Carroll MR (2013) Petrological and Volcanological Constraints on Volcanic Sulfur Emissions to the Atmosphere. In: Volcanism and the Earth's Atmosphere, vol. American Geophysical Union, pp 11-40

Shinohara H (2008) Excess degassing from volcanoes and its role on eruptive and intrusive activity. Reviews of Geophysics 46, RG4005

Shinohara H (2013) Volatile flux from subduction zone volcanoes: Insights from a detailed evaluation of the fluxes from volcanoes in Japan. Journal of Volcanology and Geothermal Research 268:46-63 doi:http://dx.doi.org/10.1016/j.jvolgeores.2013.10.007

Soden BJ, Wetherald RT, Stenchikov GL, Robock A (2002) Global Cooling After the Eruption of Mount Pinatubo: A Test of Climate Feedback by Water Vapor. Science 296(5568):727-730

Su Y, Huber C, Bachmann O, Zajacz Z, Wright H, Vazquez J (2016) The role of crystallization-driven exsolution on the sulfur mass balance in volcanic arc magmas. Journal of Geophysical Research: Solid Earth 121(8):5624-5640 doi:10.1002/2016JB013184

Tait S, Jaupart C, Vergniolle S (1989) Pressure, Gas Content and Eruption Periodicity of a Shallow, Crystallizing Magma Chamber. Earth and Planetary Science Letters 92(1):107-123

Tierney CR, Schmitt AK, Lovera OM, de Silva SL (2016) Voluminous plutonism during volcanic quiescence revealed by thermochemical modeling of zircon. Geology 44(8):683-686 doi:10.1130/G37968.1

Wallace PJ (2001) Volcanic SO2 emissions and the abundance and distribution of exsolved gas in magma bodies. Journal of Volcanology and Geothermal Research 108:85-106

Wallace PJ (2005) Volatiles in subduction zone magmas: concentrations and fluxes based on melt inclusion and volcanic gas data. Journal of Volcanology and Geothermal Research 140(1-3):217-240

Ward KM, Zandt G, Beck SL, Christensen DH, McFarlin H (2014) Seismic imaging of the magmatic underpinnings beneath the Altiplano-Puna volcanic complex from the joint inversion of surface wave dispersion and receiver functions. Earth and Planetary Science Letters 404(0):43-53 doi:http://dx.doi.org/10.1016/j.epsl.2014.07.022

White SM, Crisp JA, Spera FA (2006) Long-term volumetric eruption rates and magma budgets. Geochem Geophys Geosyst 7(doi:10.1029/2005GC001002)